Vortex pairing and reverse cascade in a simulated two-dimensional rocket motor-like flow field

Kalyana Chakravarthy and Debasis Chakraborty

Citation: Physics of Fluids **29**, 075104 (2017); doi: 10.1063/1.4989420
View online: http://dx.doi.org/10.1063/1.4989420
View Table of Contents: http://aip.scitation.org/toc/phf/29/7
Published by the American Institute of Physics

Vortex pairing and reverse cascade in a simulated two-dimensional rocket motor-like flow field

Kalyana Chakravarthy[a] and Debasis Chakraborty
Defence Research and Development Laboratory, Kanchanbagh, Hyderabad, India

(Received 24 November 2016; accepted 7 June 2017; published online 14 July 2017)

Two-dimensional large eddy simulation of a flow experiment intended for studying and understanding transition and parietal vortex shedding has brought to light some interesting features that have never been seen in previous similar simulations and have implications for future computational work on combustion instabilities in rocket motors. The frequency spectrum of pressure at head end shows a peak at the expected value associated with parietal vortex shedding but an additional peak at half this frequency emerges at downstream location. Using vorticity spectra at various distances away from the wall, it is shown that the frequency halving is due to vortex pairing as hypothesized by Dunlap *et al.* ["Internal flow field studies in a simulated cylindrical port rocket chamber," J. Propul. Power **6**(6), 690–704 (1990)] for a similar experiment. As the flow transitions to turbulence towards the nozzle end, inertial range with Kolmogorov scaling becomes evident in the velocity spectrum. Given that the simulation is two-dimensional, such a scaling could be associated with a reverse energy cascade as per Kraichnan-Leith-Bachelor theory. By filtering the simulated flow field and identifying where the energy backscatters into the filtered scales, the regions with a reverse cascade are identified. The implications of this finding on combustion modeling are discussed. *Published by AIP Publishing.* [http://dx.doi.org/10.1063/1.4989420]

I. INTRODUCTION

Transition to turbulence in solid rocket motors can have a significant effect on combustion dynamics inside solid rocket motors. Flow inside a rocket motor starts out laminar at the head end. As mass is added due to propellant burning, the flow rates increase gradually along the axis, and in cases where the motor length is long enough, it may transition to a turbulent state.[2] Velocity boundary layer has a minimal effect on the burn rate as long as there is no turbulence near the flame. When turbulence is present, it wrinkles the flame leading to increase in the overall rate of premixed gas phase reaction and the resulting heat transfer to the propellant surface. This, in turn, increases pyrolysis of the solid fuel on the propellant surface.[3] This positive feedback mechanism leads to so-called erosive burning and the nominal burning rate given by the formula $a.p^n$ (where p is the pressure and a, n are constants) has to be corrected to account for increase in the overall combustion rate.

The transition process is also important in determining the nonlinear stability of combustion in solid rocket motors. Linear stability is not sufficient to guarantee the stability of solid rocket motors. Blomshield and co-workers[4] stated that some of the motors predicted to be linearly stable can be readily pulsed into instability in motor tests. The velocity coupled response of the propellant is the primary destabilizing agent in such cases and is usually problematic when there are periods of temporary and local flow reversal near walls even if there is no mean flow separation. Such a reversal is possible if the turbulence levels grow to high levels relative to the local mean flow. If a transition to turbulence is absent or incomplete as in the case of motors with low length-to-diameter ratios, local flow reversal events are unlikely. As pointed out by Micci and co-workers,[5] it is due to this reason that motors with low length-to-diameter ratios could not be destabilized in Brownlee's experiments.[6]

Though erosive burning and velocity coupled response result from turbulence, they are seldom observed simultaneously. Erosive burning is associated with high mean flow rates which steepen the thermal boundary layer and increase heat transfer rates. Unstable combustion due to velocity coupling generally follows periods of local flow reversal at the propellant surface. For the flow to reverse easily, the mean flow should be low so that the flow can reverse the direction due to velocity fluctuations induced by turbulence and acoustics.[4] It is therefore important to understand the dependence of turbulence on the mean flow rate and other flow parameters before both these erosion effects can be modeled. The large eddy simulation (LES) presented in this paper provides a computational framework for such an effort. In order to keep the computations tractable when all the complexities associated with conjugate heat transfer, surface pyrolysis, and gas phase combustion are included, two-dimensional simulations are preferable.

Two-dimensional turbulence differs from three-dimensional turbulence due to the lack of vortex stretching, a key mechanism for generating forward energy cascade, in the former. While inertial ranges with Kolmogorov scaling are seen in both, the ones in two-dimensional turbulence are associated with backscatter, i.e., energy flows from small to large scales.[7] As a result, large scale structures that sustain for long

[a] Author to whom correspondence should be addressed: v_kalyana_chakravarthy@yahoo.co.in

periods of time are generated in two-dimensional turbulence. Given that, the implications of using two-dimensional flame-turbulence interaction simulations as models of real turbulent flames need to be studied. First task in this direction is to identify the regions of backscatter indicative of a reverse cascade process, if any, in rocket motor-like flows. If the flame is likely to be found in such regions, further research would be needed.

Flows with transpiring walls are affected by an additional feature called parietal vortex shedding that is absent in flows between solid walls. Several experimental and computational studies, some based on cold-flow emulators, have been dedicated to understanding it, after being discovered[8] in research programs associated with Ariane 5 solid booster development about two decades ago. Much of our understanding on this topic comes from the work in the following few years at ONERA. Fabignon and co-workers[9] have provided a good overview of it.

Parietal vortex shedding can occur without obstacles or convex corners in the flow due to an inherent hydrodynamic instability which is amenable to linear stability analyses.[10,11] The vortices generated are also distinct from those resulting from cross-stream injections into boundary layers from a single or an array of jets commonly used in engineering for fuel-air mixing in combustors and for surface cooling of external surfaces of supersonic/hypersonic vehicles. This instability is a characteristic of continuous injection from the wall with no discontinuities.

Resulting purely from the hydrodynamic (vortical) aspects of flows, parietal vortex shedding could, however, resonate with chamber acoustics modes leading to pressure oscillations with undesirably high amplitudes. Many studies in this area have focussed on this coupling (e.g., Refs. 9 and 12). In this context, it is also important to understand how the parietal vortices evolve subsequent to their generation. The simulation predicts a pairing process which leads to acoustic excitation at a frequency that is half of the vortex shedding frequency as in the experiment of Dunlap *et al.*[1] The effects of coherent structures resulting from the pairing process on the transition to turbulence are left out for consideration in the future.

II. NUMERICAL METHOD

Instability due to velocity coupled response is marked by the development of steep fronted shocklets resulting from steepening of compression waves.[13] In order to handle such fronts, a shock capturing scheme is needed. The levels of numerical dissipation in shock capturing schemes are too high for capturing the turbulence energy cascade efficiently. So, by themselves, these schemes are unsuitable for large eddy simulations. For LES of compressible flows, such schemes have to be hybridized with a non-dissipative scheme. For the present work, a spatially second order accurate SLAU2 shock capturing scheme[14–16] hybridized with a spatially fourth order accurate (non-dissipative) MacCormack scheme is used. An explicit second order Runge-Kutta scheme is used for temporal integration. Details of this scheme along with validation using canonical test problems can be found elsewhere[17] and are left out here for brevity. In this paper, this method is validated for transition predictions under motor-like flow conditions. The Smagorinsky model[18] is used for closing the subgrid terms that result from filtering the governing equations.

III. FLOW GEOMETRY AND CONDITIONS

The experiment of Traineau *et al.*,[19] which emulates flow in a nozzle rocket motor, is considered here. It involves flow through a rectangular duct with a closed head end and a diffuser at the other end. A schematic of the simulated geometry is shown in Fig. 1. Air is injected through porous walls at top and bottom boundaries. The injection rate is high enough for the flow to choke and become supersonic in the diffuser. The duct has a span of 40 mm in the experiment. Effects (constrictive or other) of boundary layers on solid walls in the spanwise direction have not been reported in the experimental study.[19]

Both two-dimensional and three-dimensional LESs of this flow were reported by Apte and Yang.[20,21] The former involved the simulation of only half the flow by invoking symmetric boundary conditions at the centerline. A similar two-dimensional simulation is attempted here. Three-dimensional LESs of this flow on meshes much coarser than the ones used by Apte and Yang[21] have also been reported.[22,23] Despite use of periodic boundary conditions in the spanwise direction, the first and second order statistics are accurately predicted implying that the mean flow is two-dimensional and the side wall effects are negligible. From a mean flow sense, at least, two-dimensional simulations seem justifiable.

Three-dimensional computations are certainly possible when simulating a non-reacting flow but would become intractable when surface pyrolysis and flame are included. The use of no-slip condition at the head end was reported[20] to induce a numerical artifact in the form of a recirculation zone at the injection surface and so a slip boundary condition with zero pressure gradient is used. The injected flow is normal to the porous surface and has a uniform mean with added random noise. A momentum equation in the wall-normal direction is used to compute the pressure on the porous wall while temperature of the incoming flow is uniform. The total pressure and total temperature are 3.142 atm and 260 K, respectively. The mean injection mass flux is set to 13 kg/m^{2}s which results in a mean injection velocity of about 3.1 m/s when the flow is choked. The Reynolds number based on injection velocity is about 15 000.

A 512×100 mesh is used here compared to a 640×100 mesh in the previous two-dimensional LES. Just as in the previous study, near wall resolution is set to 50 μm and stretched out away from the wall. Grid spacing is kept uniform in the axial direction. The 3D LES of Apte and Yang[21] used a

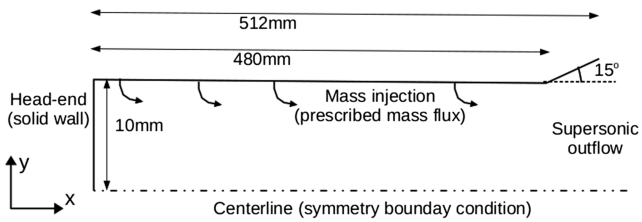

FIG. 1. Schematic of the flow geometry.

640 × 140 × 100 mesh with the same near wall grid spacing. Note that 100 points in the wall-normal direction over half channel height in both 2D simulations can provide better resolution than the 140 points used to discretize the complete channel height in 3D LES. Wasistho *et al.* have used $420 \times 64 \times 32$ meshes for their LESs.

Generally friction velocity and kinematic viscosity are used to determine wall units for length. In wall units determined this way, the near wall (wall-normal) grid spacing varies from 2 at the head end to about 12 at the nozzle.[21] However, injection velocity is an additional relevant variable in determining near transpiring-wall dynamics (and resolution requirements). The injection velocity is about 1.5 to 6 times the friction velocity in this flow. Based on earlier work, Apte and Yang[21] stated that the grid spacing in wall units need not be less than unity near transpiring walls. Injection leads to thickening of the wall layer and reduction in wall shear stress and moves the transition process away from the wall.[21] Experimental measurements[19] also showed that peaks in turbulence levels are also shifted away from the wall when compared to flows with solid walls.

The following procedure is used to initialize the flow field at the start of the simulation. Cross-sectional average properties are determined using compressible one-dimensional flow equations with source terms to account for mass addition and a choked flow condition at the start of the diffuser. Analytical velocity profile for an inviscid incompressible flow with surface mass injection is used to prescribe the shape of axial velocity profile along the wall-normal direction.[20] Density and temperature are assumed to be uniform along the wall-normal direction. Given the axial and wall-normal variations of axial velocity and density, the wall-normal velocity field is determined by assuming that the initial momentum vector is divergence-free. Flow-through time is determined based on velocity that is one-half of sonic speed and length of the constant area section. After an initial transient of about 8 flow-through times, statistics corresponding to a stationary state are computed over 10 flow-through times.

IV. RESULTS

The predicted lateral profiles of mean axial velocities at several axial locations are compared to corresponding profiles from reference LES[20] and experimental[19] data in Fig. 2. The velocity profiles tend to flatten out near the centerline indicating a transition from a laminar to turbulent state as the flow approaches the exit. In fact, at the first location, the predicted and experimental profiles are indistinguishable from a laminar profile. At the fourth axial location, there is clear deviation from a laminar state. Both LESs predict very similar results except at one of the locations and this could be due to slight difference in predictions of the transition location.

The axial profiles of mean axial velocity on the centerline and a location closer to the porous wall are shown in Fig. 3. On the centerline, LES predicts a faster growth of axial velocity with distance compared to the experiment, while the opposite seems to be true close to the wall. For a given mass flux, the velocity on the centerline would be lower if the flow is turbulent due to a more uniform distribution of the flow. At locations close to the wall, velocity would be higher if the flow is turbulent than if it is laminar. Figure 3 indicates that the transition to turbulence, which leads to a more even distribution of the flow, is delayed in both simulations when compared to experiments. This is despite the fact that a random component of incoming mass flux at the porous wall was specified to be nearly 90% of the deterministic component by Apte and Yang.[20] This delay is, therefore, not due to the lack of sufficient triggering. Transition prediction using LES is tricky due to the fact that many subgrid models are derived for fully developed turbulence and are not accurate for transition. It is known that adopting dynamic filtering leads to better predictions for transition when compared to those made using the baseline subgrid model.[24] More sophisticated models may improve the predictions but the fact remains that two-dimensional simulations cannot capture certain mechanisms like vortex stretching and hairpin vortices which play a significant role in the transition of wall bounded flows, and so some deviation from the experimental behavior should always be acceptable.

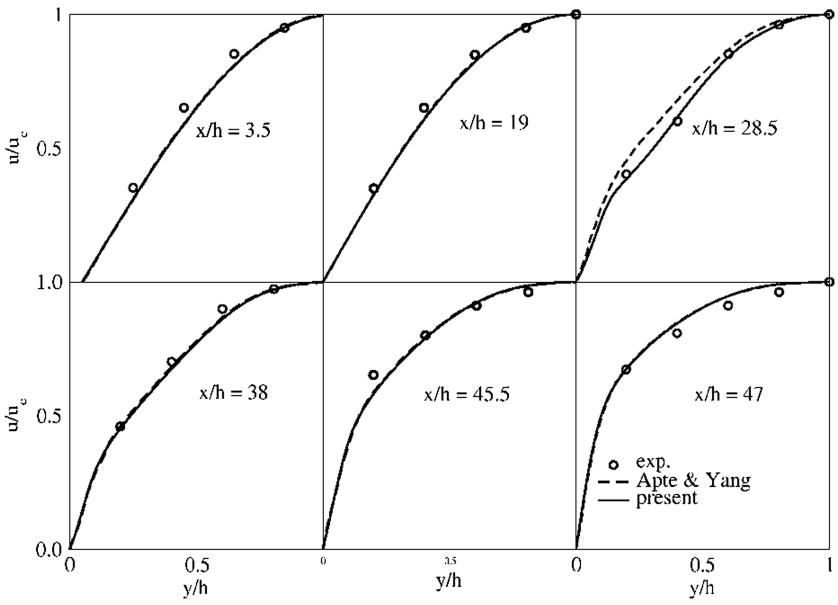

FIG. 2. Mean streamwise velocity profiles (non-dimensionalized using corresponding local centerline value, u_c). "h" is the half height of the channel.

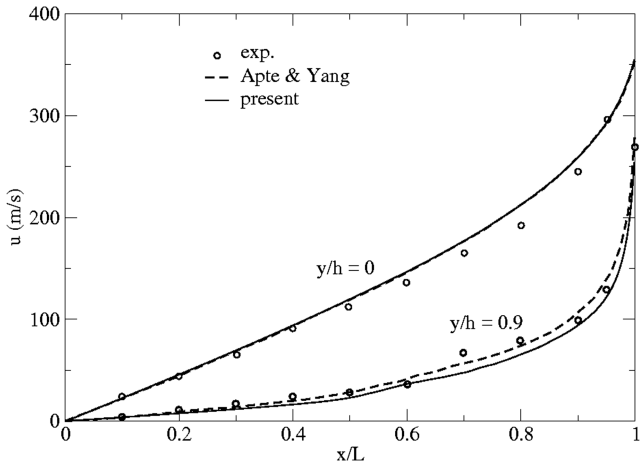

FIG. 3. Axial variations of mean streamwise velocity profiles on the centerline and at near wall locations. "L" is the length of the rectangular portion.

The frequency spectra of axial velocity at various axial locations are plotted in Fig. 4. The emergence of broadband and more energetic spectra is evident as the flow approaches the exit and transitions to a turbulent state. Inertial range with a power law scaling with an exponent of −5/3 also becomes evident. It is also observed although a little less evident in the spectra computed from the LES of Apte and Yang.[20]

Kraichnan-Leith-Batchelor (KLB) theory[7,25,26] predicts an enstrophy inertial range with a power law scaling with an exponent tending to −3 in the high Reynolds number limit in addition to the energy inertial range with the Kolmogorov scaling in two-dimensional turbulence. This additional inertial range has been reported to be associated with the existence of coherent vortex structures. It is absent in three-dimensional turbulence perhaps due to the fact that vortex stretching which leads to bending of vortex tubes/filaments and eventual breakdown into three-dimensional turbulence. In essence, two-dimensional coherent vortices are relatively short-lived in three-dimensional turbulence. The spectra at downstream locations (see Fig. 4) actually show both scalings in different frequency bands. However, unlike in the case of forced isotropic turbulence for which KLB was originally derived, the enstrophy inertial range is at lower frequencies (wavenumbers) when compared to the inertial range.

The enstrophy inertial range is associated with transfer of enstrophy from larger to smaller scales (forward scatter), and in cases where enstrophy is injected at large scales, it can form to the left of the energy inertial range. In fact, atmospheric boundary layers which are sufficiently two-dimensional exhibit this kind of behavior.[27] The evidence for the opposite behavior (enstrophy inertial range to the right of inertial range) comes from relatively recent two-dimensional high resolution simulations,[28] and to authors' knowledge, there is no experimental evidence reported in the literature. The stochastic forcing in their simulation in a wavenumber band sets up a forward enstrophy cascade to the right while kinetic energy cascades up on its left. In wavenumber/frequency domain, the enstrophy inertial range can, therefore, form either to the left or to the right of the energy inertial range depending on where the energy in injected. In the present work, the energy addition (white noise at the porous wall) is distributed evenly at all resolved scales of the simulation.

The present LES has sufficient resolution for capturing both the enstrophy inertial range (presumably generated by the injection of enstrophy by large scale coherent vortices generated by hydrodynamic instability at the injection surface) and the energy inertial range at the last two axial locations. The enstrophy inertial range is generated at the second axial location due to the presence of coherent vortices but the inertial range is still missing at this location. The energy cascade with inertial range Kolmogorov scaling is established only at locations further downstream. It is worth checking if inertial range Kolmogorov scaling is associated with a reverse energy cascade given that it is expected in two-dimensional turbulence if the Reynolds number is sufficiently high.

The non-homogeneous nature of the flow makes proper orthogonal decomposition like spectral analysis and

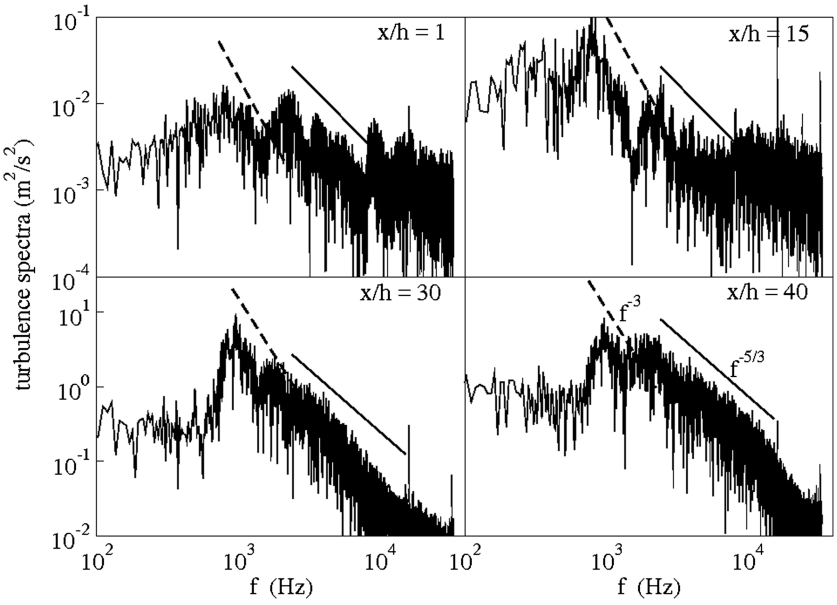

FIG. 4. Turbulence spectra at various axial locations.

computation of energy flux across a given length scale difficult. The spatial filtering operation provides an alternative way of checking for energy backscatter within the resolved scales. Borrowing the idea of test filtering from the literature related to dynamic filtering large eddy simulation approaches,[24] a test filter with width that is double the grid spacing along each direction is defined and the velocity field is Favre filtered as follows:

$$\langle u_i \rangle = \frac{\overline{\rho u_i}}{\overline{\rho}}. \tag{1}$$

$\overline{\phi}$ here presents spatial filtering using the test filter of any dependent variable ϕ resulting from the simulation. The subfilter stress $\overline{\rho}(\langle u_i \rangle \langle u_j \rangle - \langle u_i u_j \rangle)$ contracted with the filtered strain rate, $\langle S_{ij} \rangle$, results in the energy transfer to the scales that are filtered out. A negative value indicates that energy flows from the scales that are smaller than the filter width to those that are larger and indicated backscatter within scales captured in the simulation. A grayscale map of this quantity with marked isolevels of this quantity within the rectangular portion of the domain is shown in Fig. 5. At the downstream end where transition is complete, turbulence is likely fully developed; there is a reverse cascade of kinetic energy in the core region. The turbulence in this area is more isotropic and unaffected by the near wall dynamics dominated by viscous terms and therefore exhibits a behavior expected from two-dimensional classical theories for homogeneous isotropic turbulence.

Flame-turbulence interactions in many of the past studies (e.g., Refs. 29 and 30) have relied on two-dimensional simulations. Even with current day computational power, the choice has to be made between two-dimensional simulations with detailed chemistry and three-dimensional simulations with simplified chemistry even for laboratory flames.[31] Three-dimensional simulations at Reynolds numbers high enough to be relevant in engineering remain out of reach even with simple chemistry models.

Statistical characterizations of the flame surfaces in three-dimensional simulations using probability density functions of quantities such as the local shape factor, flame orientation relative to the principle direction of strain rate, and vorticity in several studies[32,33] have shown that premixed flames tend to wrap around cylindrical vortex filaments and the local shape is mostly cylindrical rather than spherical or saddle-like. Given that, it has been assumed that (simulated) two-dimensional turbulent flames are sufficiently close to three-dimensional counterparts. A comparative study of two-dimensional and

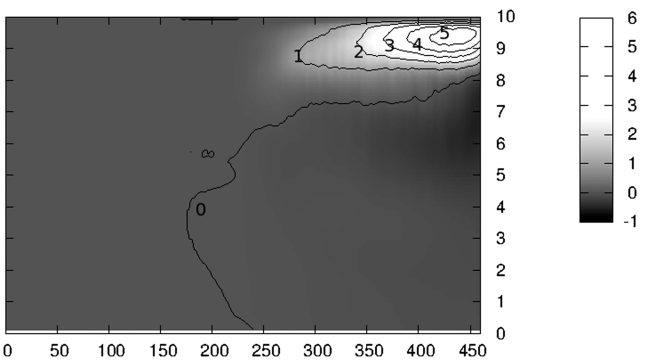

FIG. 5. Grayscale map of energy flux from the filtered field.

three-dimensional large eddy simulation approaches for premixed turbulent flames by Ibrahim and co-workers[34] sought to identify situations where such an assumption would be invalid. The tendency of two-dimensional turbulence to create large, long-lived flow structures due to the reverse energy cascade process has seldom been noted in two-dimensional flame simulation studies. Search for a reverse cascade, if any, in this study started out as an effort to understand its implications when modeling the flame in the context of solid rocket motors. Figure 5 suggests that there is actually no need for such an effort since the near wall region does not have a reverse cascade. The flame would be confined to the region with forward energy scatter. In actual solid rocket motors where the pressures are much higher, the flame would be even closer to the propellant surface. The predictions of turbulence levels in the near wall regions are however key to capturing the flame dynamics.

The predictions of turbulent kinetic energy at various axial locations are compared to corresponding experimental data in Fig. 6. LESs seem to capture the increase in fluctuations associated with laminar-to-turbulent transition. Both LESs predict nearly similar results except at the last axial location where the present LES captures the near wall peak in turbulence intensity slightly better. The predicted peaks in the profiles are closer to the wall than those in the experiment but the peak values are well predicted. The turbulence intensities in the core region are overpredicted, which is likely due to the reverse cascade process or reduction of turbulent kinetic energy dissipation resulting from the use of symmetry boundary conditions. As in the case of experiments in a cylindrical motor geometry with wall injection,[1] the peak and centerline values stabilize to constant values once the transition is complete. As in this study, there is a slow spreading of turbulence kinetic energy towards the centerline.

The frequency spectra of pressure fluctuations near the wall (y/h = 0.9) at four axial locations are shown in Fig. 7. Due to an open boundary condition at the exit of the rectangular chamber, no acoustic standing waves are evident. The pressure fluctuations are associated with vorticity fluctuations in the boundary layer. In the upstream laminar regions, there are minimal vorticity fluctuations and so only a single peak corresponding to vortex shedding associated with hydrodynamic instability is seen at a frequency of 1806 Hz. As the vorticity fluctuations grow with the onset of transition, more broadband spectra are seen close to the exit.

There is a noteworthy difference in pressure predictions of the two LESs. At the two downstream locations, broad peaks around 900 Hz are seen in the present LES. The LES of Apte and Yang[20] does not predict these peaks. The peak always seems to be around 1800 Hz which is attributed to parietal vortex shedding. This frequency is inline with the Strouhal number expected from earlier literature on parietal vortex shedding.[35]

The experiment of Dunlap and co-workers[1] is quite similar to the one being simulated here. It involves a cylindrical motor geometry instead of a rectangular one. Observations from this experiment suggested that vortices generated at the wall paired up as they moved away into the core flow resulting in frequency halving. It is possible that the pairing process could also be happening in the present LES. To verify this hypothesis, frequency spectra of vorticity at various

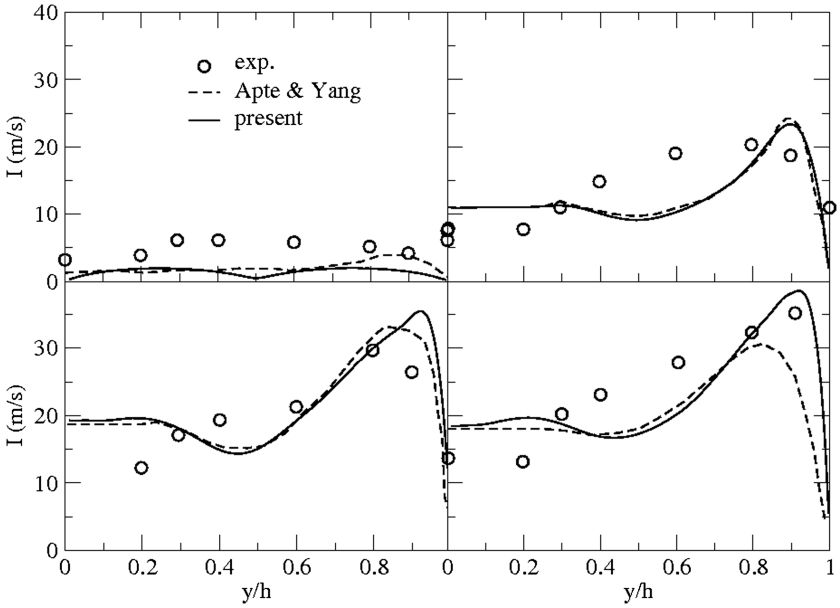

FIG. 6. Predictions of turbulence levels at various axial locations.

distances away from the wall and the x/h = 30 axial location are computed and plotted in Fig. 8. Near the wall, the peak in spectra corresponds to parietal vortex shedding frequency near 1800 Hz. As the flow moves away from the wall, the pairing process starts and a peak at half this frequency starts to emerge. Beyond a certain distance, the pairing process is complete and only the new peak around 900 Hz is evident. Further away from the wall, an almost potential core of the flow has very low amplitude fluctuations which are perhaps associated with chamber modes.

Whether the parietal vortices in reality remain two-dimensional long enough to pair up remains a somewhat open question given that the present simulation is two-dimensional. For example, bending of these large structures to form hair-pin vortices is not possible in the present simulation. While conclusive evidence would have to come from either experimental measurements (as in the study of Dunlap *et al.*[1]) or a three-dimensional simulation, the three-dimensional LES of Apte and Yang[21] sheds some light on this issue. It predicts coherent, 2-dimensional vortex structures that persist till x/h = 35 and then break down generating 3-dimensional smaller eddies. The formation of these structures which are not found in channel flows with solid walls has been attributed to the prevention of high-speed outer fluid penetration into the near wall region due to injection.

While the observed process of 2-dimensional structures breaking down into 3-dimensional turbulence appears to be the Tollmien-Schlichting (T-S) route to transition, it is unlikely, given the high level of noise injection. In such cases, the bypass route is expected. Here, pairing is demonstrated at x/h = 30 which is before the breakdown location. The Tollmien-Schlichting (T-S) waves are also much weaker than the parietal vortices generated by surface injection. The latter also have a distinct frequency of shedding. T-S waves/structures have

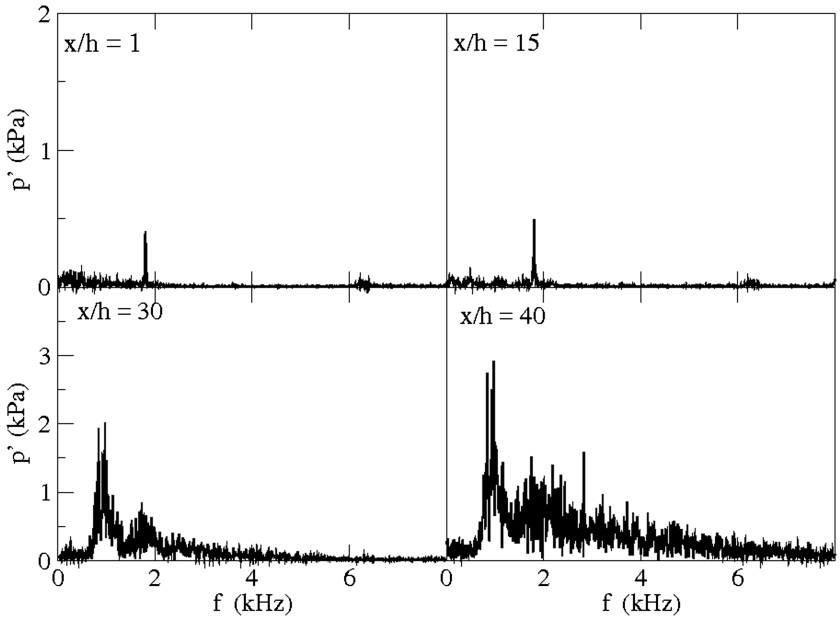

FIG. 7. Frequency spectra of pressure at various axial locations.

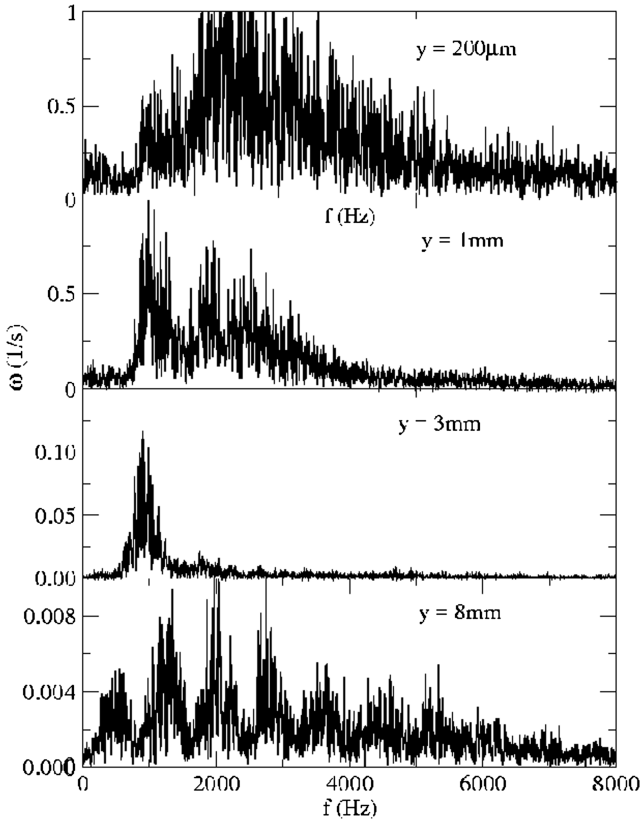

FIG. 8. Frequency spectra of vorticity at various axial locations.

never been shown to be strong enough to couple with chamber acoustic modes to cause resonance. Parietal vortex shedding, on the other hand, was discovered in rocket motors mostly due to the strong influence that they have on acoustics.

V. CONCLUSIONS

A two-dimensional simulation of a flow experiment designed to study and understand parietal vortex shedding and acoustics in solid rocket motors has been performed. Pairing of vortices resulting from intrinsic instability associated with wall injection (parietal vortex shedding) is observed as in the experimental study of Dunlap and co-workers.[1] Though both two-dimensional[36,20] and three-dimensional LESs[21–23] of this flow have been reported, such pairing was either not captured or remained unnoticed.

The Kolmogorov spectrum in two-dimensional turbulence is associated with energy inertial range where the kinetic energy backscatters from smaller to larger scales.[7,25,26] The two-dimensional LES, past and present, clearly indicates the Kolmogorov scaling for the velocity spectra. A way of checking for a possible reverse cascade has been proposed and used to confirm that such a process is indeed captured within resolved scales in the fully turbulent portion of the flow. This process is, however, in the core region of the flow and not near the wall region where the gas phase flame in rocket motors is likely to be. The intensity of near wall turbulence, which the flame is likely to encounter, has been accurately captured like in past LESs and so the current approach can be considered for future work involving flame-turbulence interactions.

The coupling between acoustics and laminar-to-turbulence transition has also been studied almost separately[37–39] even before parietal vortex shedding was discovered. The present work also deals separately with observations related to parietal vortex shedding and transition/turbulence. The effect of parietal vortex shedding, with or without the pairing process, on transition remains unexplored.

[1] R. Dunlap, A. M. Blackner, R. C. Waugh, J. R. S. Brown, and P. G. Willoughby, "Internal flow field studies in a simulated cylindrical port rocket chamber," J. Propul. Power **6**(6), 690–704 (1990).
[2] B. Gazanion, F. Chedevergne, X. de Saint-Victor, J.-L. Estivalezes, and G. Casalis, "Laminar-turbulent transition investigation in a solid rocket motor representative cold flow setup," AIAA Paper 2013-3918, 2013.
[3] K. O. Sabdenov, "On the threshold nature of erosive burning," Combust. Explosion Shock Waves **44**(3), 300–309 (2008).
[4] F. Blomshield, H. Mathes, J. Crump, C. Beiter, and M. Beckstead, "Nonlinear stability testing of full-scale tactical motors," J. Propul. Power **13**(3), 356–366 (1997).
[5] R. Glick, M. Micci, and L. Caveny, "Transition to nonlinear instability in solid propellant rocket motors," AIAA Paper No. 81-1520, 1981.
[6] W. Brownlee, "Nonlinear axial combustion instability in solid propellant motors," AIAA J. **2**(2), 275–284 (1964).
[7] R. H. Kraichnan, "Inertial ranges in two-dimensional turbulence," Phys. Fluids **10**, 1417–1423 (1967).
[8] N. Lupoglazoff and F. Vuillot, "Parietal vortex shedding as a cause of instability for long solid propellant motors–Numerical simulations and comparison with firing tests," AIAA Paper No. 96-0761, 1996.
[9] Y. Fabignon, J. Dupays, G. Avalon, F. Vuillot, N. Lupoglazoff, G. Casalis, and M. Prevost, "Instabilities and pressure oscillations in solid rocket motors," Aerosp. Sci. Technol. **7**(3), 191–200 (2003).
[10] F. Chedevergne, G. Casalis, and J. Majdalani, "Direct numerical simulation and biglobal stability investigations of the gaseous motion in solid rocket motors," J. Fluid Mech. **706**, 190–218 (2012).
[11] G. Boyer, G. Casalis, and J. L. Estivalezes, "Stability analysis and numerical simulation of simplified solid rocket motors," Phys. Fluids **25**, 084109 (2013).
[12] A. Kourta, "Instability of channel flow with fluid injection and parietal vortex shedding," Comput. Fluids **33**, 155–178 (2004).
[13] P. Hughes and A. Saber, "Nonlinear combustion instability in a solid propellant two-dimensional window motor," AIAA Paper No. 78-1008, 1978.
[14] E. Shima and K. Kitamura, "On new simple low-dissipation scheme of AUSM-family for all speeds," AIAA Paper 2009-136, 2009.
[15] K. Kitamura and E. Shima, "Improvements of simple low-dissipation AUSM against shock instabilities in consideration of interfacial speed of sound," in 5th European Conference on Computational Fluid Dynamics, ECCOMAS CFD, Lisbon, Portugal, 2010.
[16] V. K. Chakravarthy and D. Chakraborty, "Modified SLAU2 scheme with enhanced shock stability," Comput. Fluids **100**, 176–184 (2014).
[17] V. K. Chakravarthy, K. Arora, and D. Chakraborty, "A simple hybrid finite volume solver for compressible turbulence," Int. J. Numer. Methods Fluids **77**(12), 707–731 (2015).
[18] J. Smagorinsky, "General circulation experiments with the primitive equations," Mon. Weather Rev. **91**, 99–110 (1963).
[19] J. C. Traineau, P. Hervat, and P. Kuentzmann, "Cold-flow simulation of a two-dimensional nozzleless solid-rocket motor," AIAA Paper No. 86-1447, 1986.
[20] S. Apte and V. Yang, "Unsteady flow evolution is porous chamber with surface mass injection. Part I: Free oscillations," AIAA J. **39**(8), 1577–1586 (2001).
[21] S. V. Apte and V. Yang, "A large-eddy simulation study of transition and flow instability in a porous-walled chamber with mass injection," J. Fluid Mech. **477**, 215–225 (2003).
[22] B. Wasistho, S. Balachandar, and R. Moser, "Compressible wall-injection flows in laminar, transitional, and turbulent regimes: Numerical prediction," J. Spacecr. Rockets **41**(6), 915–924 (2004).
[23] B. Wasistho and R. Moser, "Simulation strategy of turbulent internal flow in solid rocket motor," J. Propul. Power **21**(2), 251–263 (2005).
[24] M. Germano, U. Piomelli, P. Moin, and W. H. Cabot, "A dynamic subgrid-scale eddy viscosity model," Phys. Fluids A **3**(7), 1760–1765 (1991).

[25]C. E. Leith, "Diffusion approximation for two-dimensional turbulence," Phys. Fluids **11**, 671–673 (1968).
[26]G. K. Batchelor, "Computation of the energy spectrum in homogeneous two-dimensional turbulence," Phys. Fluids **12**, 233–239 (1969).
[27]E. Gkioulekas and K. Tung, "Recent developments in understanding two-dimensional turbulence and the Nastrom-Gage spectrum," J. Low Temp. Phys. **145**, 25–57 (2006).
[28]M. M. Farazmand, N. K. R. Kevlahan, and B. Protas, "Controlling the dual cascade of two-dimensional turbulence," J. Fluid Mech. **668**, 202–222 (2011).
[29]M. Baum, T. J. Poinsot, D. C. Haworth, and N. Darabiha, "Direct numerical simulation of $H_2/O_2/N_2$ flames with complex chemistry in two-dimensional turbulent flows," J. Fluid Mech. **281**, 1–32 (1994).
[30]N. Peters, P. Terhoeven, J. H. Chen, and T. Echekki, "Statistics of flame displacement speeds from computations of 2-D unsteady methane-air flames," Proc. Combust. Inst. **27**, 833–839 (1998).
[31]N. Chakraborty, M. Klein, and R. S. Cant, "Effects of turbulent Reynolds number on the displacement speed statistics in the thin reaction zones regime of turbulent premixed combustion," J. Combust. **2011**(473679), 1–19.
[32]I. Shepherd and W. Ashurst, "Flame front geometry in premixed turbulent flames," Proc. Combust. Inst. **24**(1), 485–503 (1992).
[33]V. K. Chakravarthy and S. Menon, "Subgrid modeling of turbulent premixed flames in the flamelet regime," Flow, Turbul. Combust. **65**, 131–161 (2001).
[34]S. S. Ibrahim, A. M. S. Ali, and A. R. Masri, "Two-versus three-dimensional LES of premixed turbulent propagating flames," in Third Symposium on Turbulence and Shear Flow Phenomena, Sendai, Japan, 2003.
[35]B. Ugurtas, G. Avalon, N. Lupoglazoff, and G. Casalis, "Stability and acoustic resonance of internal flows generated by side injection," in *Solid Propellant Chemistry, Combustion and Motor Internal Ballistics*, Progress in Astronautics and Aeronautics (AIAA, New York, 2000), Vol. 185.
[36]T.-M. Liou, W.-Y. Lien, and P.-W. Hwang, "Transition characteristics of flowfield in a simulated solid-rocket motor," J. Propul. Power **14**(3), 282–289 (1988).
[37]R. Beddini and T. Roberts, "Turbularization of an acoustic boundary layer on a transpiring surface," AIAA Paper No. 86-1448, 1986.
[38]Y. Lee and R. A. Beddini, "Effect of solid rocket chamber pressure on acoustically-induced turbulent transition," AIAA Paper 2000-3802, 2000.
[39]S. Apte and V. Yang, "Unsteady flow evolution is porous chamber with surface mass injection. Part II: Forced oscillations," AIAA J. **40**(22), 244–253 (2001).